Computer-simulation studies of diskotic liquid crystals

Habtamu Zewdie*
Department of Chemistry, University of Southampton, Southampton SO17 1BJ, England
(Received 12 May 1997)

We have developed a single site anisotropic pair potential suitable for computer-simulation studies of systems composed of disklike molecules. The general dependence of the potential on the intermolecular separation is taken to be the shifted 12-6 Lennard-Jones form. The range and strength parameters in the potential depend on the orientations of the molecules and that of the intermolecular vector, as introduced by Corner; we propose that the form of this dependence may be represented by an S-function expansion. A hard oblate spherocylinder with a shape anisotropy $(D+L)/L$ of 3, where D is the diameter of the cylinder with length L, is considered to be a more realistic model for disklike molecules. The expansion coefficients for the range parameter were determined by mapping the expansion onto a set of center of mass separations at the closest approach of a pair of such disks. Each term in the expansion of the strength parameter can be associated with a specific type of interaction: isotropic, anisotropic (nematic favoring, columnar favoring, smectic favoring), and quadrupolar (tilt favoring). This allows fine tuning of each coefficient in the expansion of the strength parameter to reflect the relative strength of a specific type of interaction. To facilitate comparison with studies of the more successful Gay-Berne (GB) potential model, we have determined the expansion coefficients for the strength parameter by mapping the expansion onto that of the GB model. To explore the value of the model potential for studies of diskotic liquid crystals, we have carried out a detailed Monte Carlo simulation at a packing fraction (Nv_0/V) of 0.55. The system was found to exhibit isotropic, diskotic-nematic (N_D), diskotic-columnar $(D'_{\mathrm{ho}},D_{\mathrm{ho}},D_{\mathrm{hd}})$, and crystal phases. The effect of temperature, density, and the form of the attractive contribution to the potential on the phase stability and the nature of the transitions between the diskotic mesophases is investigated. Such phase behavior contrasts with those for a system of hard oblate spherocylinders and for cut hard spheres with the same shape anisotropy which only form isotropic and crystalline phases and the GB model, which has difficulty in forming columnar phases. Spherical harmonics can be evaluated efficiently by computers. This makes our model potential computationally cheaper.
[S1063-651X(98)11102-9]

PACS number(s): 61.30.Cz, 64.70.Md, 83.70.Jr, 61.25.Em

I. INTRODUCTION

Liquid crystals formed from disk-shaped molecules were first reported in 1977 [1]. Since then these phases have been studied extensively [2–8]. However, theoretical studies of systems composed of disklike molecules are fairly limited [6–7]. The discovery of diskotic mesophases has initiated simulation of such systems. A fluid of hard oblate spherocylinders has been studied to serve as a reference system in a perturbation theory of a fluid composed of disk-shaped molecules [9,10]. Models based on thin hard platelets [11] and oblate ellipsoids [12–14] appear to form only diskotic-nematic and isotropic phases. A cut hard sphere has been proposed as a model for disklike mesogens [15]. The simulation of the system composed of cut hard spheres showed a rich polymorphism (diskotic-columnar, diskotic-nematic, cubatic, and isotropic phases). These results show that repulsive forces alone are able to explain liquid crystalline behavior for systems of disklike molecules although the thermotropic nature of the transitions for real systems is clearly missing from the model.

The molecules which form diskotic mesophases are flat (a benzene ring, or a system of condensed rings) surrounded more or less symmetrically by alkyl chains. The nature of the mesophases formed from such molecules depends on the delicate balance between the short-range repulsion, the long-range attraction, and the flexibility of the chains attached to the disk. In addition, it is known that attractive forces are able to stabilize phases not observed with hard particle models alone. Systems composed of rodlike molecules interacting with both short-range repulsion and long-range attraction have been studied often by computer simulation, whereas studies for disklike molecules are rather scarce. Potential models for simulating diskotic systems which account for both the short-range repulsion and long-range attraction have been proposed. In these models the long-range part has been modeled using the attractive part of the Gay-Berne (GB) potential suitably parametrized to reflect oblate ellipsoid symmetry. The short-range repulsive part has been modeled as a sphere [16] and as an oblate ellipsoid [17]. The model based on a spherical core is reported to form isotropic, diskotic-nematic, columnarlike, and crystal phases on cooling. The model based on an oblate ellipsoid is reported to exhibit isotropic, diskotic-nematic and, depending, on the density rectangular (D_{ro}) or hexagonal columnar (D'_{ho}) phases. However, the disks in the neighboring columns are reported to show strong correlations. Such translationally correlated structures may be considered as layerlike. The longitudinal pair distribution function $g_{\|}(r^*_{\|})$ determined in the columnar phase for the spherical model shows oscillations with a peak spacing comparable to the molecular dimensions typical of smectic phases. This contrasts with that found for the colum-

*Permanent address: Department of Chemistry, Addis Ababa University, P.O. Box 1176, Addis Ababa, Ethiopia.

nar phase formed from ellipsoids, which shows a periodicity of half the molecular thickness in the longitudinal pair distribution function. We argue that, from the pair distribution functions $g(r^*)$, $g_\parallel(r_\parallel^*)$, and $g_\perp(r_\perp^*)$ alone, it is difficult to establish conclusively if the translationally ordered phase is a columnar, a smectic, a crystal precursor or a crystal phase. In general it is difficult to crystallize such systems by cooling. This makes it difficult to establish the equilibrium structure of the translationally ordered phase at low temperatures.

The formation of columnar phases by hard oblate ellipsoids of revolution are ruled out based on scaling arguments [18,19]. However, the suitably parametrized GB potential is expected to form a columnar order. A face-to-face configuration of parallel disklike molecules is more stable than a side-by-side configuration. Such potentials favor the formation of a columnar phase. However, excluded volume effects appear to favor the diskotic-nematic phase over the columnar phase. This result has implication on whether an oblate ellipsoid with a suitably parametrized GB potential could form various types of columnar phases. The result reported in Ref. [17] indicates that it is difficult for models based on an oblate ellipsoid to form a columnar phase of the type $D_{\rm hd}$. The thick middle region of the ellipsoid together with its relatively tapered edge appear to make the formation of columnar phases difficult, and are more in favor of the diskotic-nematic phase. This effect is enhanced as the shape anisotropy decreases. Similar behavior has been observed in the different but related system of prolate ellipsoids, with the length-to-breadth ratio set equal to 3 and allowed to interact with GB potential for two of the parameters $\mu=2$, $\nu=1$ and $\mu=1$, $\nu=2$, in the density of interest. The attractive part of the potential together with the ellipsoidal shape appears to favor the nematic phase over the smectic-A phase [20,21].

In this paper we have developed a pair potential suitable for computer-simulation studies of systems composed of disklike molecules, and so favor the formation of diskotic-columnar phases following that which we developed to study rodlike molecules and showed to exhibit a rich polymorphism [21]. The pair potential is assumed to have the shifted Lennard-Jones 12-6 form [22]. The range and strength functions in the potential are expanded in a complete orthogonal basis set of S functions. A hard oblate spherocylinder is considered to be a more realistic model for disklike molecules. The expansion coefficients for the range parameter were estimated by mapping the expansion onto a set of center of mass separations at closest approach of a pair of such disks. The potential strength parameter is also expanded in the basis set of S functions. Each term in the expansion of the strength parameter reflects a specific type of interaction as isotropic, anisotropic (nematic favoring, columnar favoring, smectic favoring), and quadrupolar (tilt favoring), thus allowing us to fine tune each coefficient to reflect the relative strength of a specific type of interaction. In this work we have determined the expansion coefficients for the strength parameter by mapping the expansion onto the GB strength parameter for disklike molecules. This has enabled us to make a direct comparison with studies made on similar attractive but different repulsive interactions. We have performed a detailed Monte Carlo simulation study of the different phases formed for the chosen model potential.

The plan of the paper is as follows. In Sec. II we will describe the model potential and its parametrization. The computational details of the Monte Carlo simulation is described in Sec. III. In Sec. IV we present the results and our discussion of them. Conclusions are given in Sec. V.

II. PAIR POTENTIAL

The shifted form of the Lennard-Jones 12-6 potential [22] has proved successful in computer-simulation studies of anisotropic molecular interactions [16,17,21,23], and is given as

$$U(\hat{u}_1,\hat{u}_2,\mathbf{r})=4\epsilon(\hat{u}_1,\hat{u}_2,\hat{r})\left[\left(\frac{\sigma_0}{r-\sigma(\hat{u}_1,\hat{u}_2,\hat{r})+\sigma_0}\right)^{12}-\left(\frac{\sigma_0}{r-\sigma(\hat{u}_1,\hat{u}_2,\hat{r})+\sigma_0}\right)^{6}\right], \tag{1}$$

where σ_0 is a distance scaling parameter. The unit vectors $\hat{u}_1$ and $\hat{u}_2$ define the molecular orientations, and $\hat{r}$ defines the intermolecular vector orientation. $\sigma(\hat{u}_1,\hat{u}_2,\hat{r})$ and $\epsilon(\hat{u}_1,\hat{u}_2,\hat{r})$ are the potential range and strength parameters, respectively. The distance $r=\sigma(\hat{u}_1,\hat{u}_2,\hat{r})$ is the separation at which the repulsive and attractive components of the potential exactly balance, and $\epsilon(\hat{u}_1,\hat{u}_2,\hat{r})$ is the potential well depth for given molecular and intermolecular vector orientations. The challenge in developing a suitable potential for computer simulation studies of disklike molecules lies in determining the molecular and intermolecular vector orientations dependence of the two main parameters in the Lennard-Jones potential: the range parameter $\sigma(\hat{u}_1,\hat{u}_2,\hat{r})$ and the strength parameter $\epsilon(\hat{u}_1,\hat{u}_2,\hat{r})$. The $\hat{r}$, $\hat{u}_1$, and $\hat{u}_2$ dependence of the strength and range parameters have been defined to take various forms following the pioneering work of Corner [24]. Berne and Pechukas [25] introduced the overlap model to estimate the range and strength parameters analytically as the ones which define the overlap integral of two ellipsoidal Gaussians. However, the most studied model is the modified overlap potential proposed by Gay and Berne [22] for studies of systems composed of prolate ellipsoids. The GB potential model was parametrized and used for computer simulation studies of systems composed of oblate ellipsoids representing diskotics [17], and appears to favor the formation of highly interdigitated columnar phases. Consequently the formation of the diskotic-nematic phase appears to be favored over the diskotic-columnar phase. An oblate spherocylinder is argued to be probably a more realistic model to study the structure and thermodynamic properties of systems composed of disklike molecules. We, therefore chose an oblate spherocylinder with diameter to thickness ratio $(D+L)/L$ equal to 3 to represent the shape of a diskogen. An oblate spherocylinder of width $D+L$ and thickness L can be described as a ring-doughnut shape of cylinder diameter L and middle-loop diameter D, where a cylindrical cut of diameter D along the middle of the loop is replaced with a solid cylinder of diameter D and length L. We used the S-function expansion formalism to define the molecular and intermolecular vector orientations dependence of the range as well as the strength functions [21]. The first six S functions [26] used for expansion are presented in Table I.

TABLE I. The first six S functions [26]. Here $\hat{u}_1$, $\hat{u}_2$, and $\hat{r}$ are unit vectors defining the orientations of the molecules and the intermolecular vector, respectively. All orientations are defined in an arbitrary laboratory frame and we use the following definitions: $f_0=\hat{u}_1\cdot\hat{u}_2$, $f_1=\hat{u}_1\cdot\hat{r}$, and $f_2=\hat{u}_2\cdot\hat{r}$.

$S_{000}=1$, $S_{202}=(3f_1^2-1)/2\sqrt{5}$, $S_{022}=(3f_2^2-1)/2\sqrt{5}$,
$S_{220}=(3f_0^2-1)/2\sqrt{5}$, $S_{222}=(2-3f_1^2-3f_2^2-3f_0^2+9f_1f_2f_0)/\sqrt{70}$
$S_{224}=(1+2f_0^2-5f_1^2-5f_2^2-20f_0f_1f_2+35f_1^2f_2^2)/4\sqrt{70}$

A. Range function

The range function $\sigma(\hat{u}_1,\hat{u}_2,\hat{r})$ for a pair of identical cylindrically symmetric particles is expanded in the basis set of S functions as

$$\sigma(\hat{u}_1,\hat{u}_2,\hat{r})=\sigma_0[\sigma_{000}S_{000}+\sigma_{cc2}(S_{202}+S_{022})+\sigma_{220}S_{220}+\sigma_{222}S_{222}+\sigma_{224}S_{224}], \quad (2)$$

where σ_0 is a distances scaling parameter and σ_{000}, σ_{cc2}, σ_{220}, σ_{222}, and σ_{224} are the five expansion coefficients. Configurations of a pair of particles which were considered to be important to reproduce the shape of the particles and give a good estimate of the expansion coefficients were identified. For each configuration the minimum distance of approach between a pair of molecules was determined, say σ_i. The more general least squares objective function χ^2_σ was defined as

$$\chi^2_\sigma=\sum_{i=1}^{N} w_i[\sigma_i-\sigma(\hat{u}_1,\hat{u}_2,\hat{r})]^2, \quad (3)$$

where w_i is a weighting function for the ith configuration, and N is the number of configurations identified. We have considered up to 33 configurations to reproduce the shape of interest. The expansion coefficients were determined as those which minimized χ^2_σ. It is important to judge the quality of the fit, particularly for the range function, by the magnitude of the error function as well as visual inspection of the resulting geometry. The quality of the fit judged simply by the magnitude of the error function can be quite misleading, as an acceptable error function could result in a completely undesirable geometry. In this exercise the absolute error in the width and thickness of the spherocylinder was 0.001. The overall comparison is given in Fig. 1. The coefficients determined by this procedure are summarized in Table II. The negative sign of the three coefficients σ_{cc2}, σ_{220}, and σ_{222} shows that the end-to-end and perpendicular orientations of molecules are important in determining the range parameter. The coefficient of S_{224} for the range parameter shows a large positive value indicating that the shape anisotropy behaves like a quadrupolar effect.

In Fig. 1 we present comparisons of the range parameter, $\sigma^*=\sqrt{x^{*2}+y^{*2}}$, and the shape of the excluded volume (the region bounded by the points satisfying the condition $\sigma^*=\sqrt{x^{*2}+y^{*2}}$. σ^* for the hard oblate spherocylinders was determined numerically; for our model it was obtained via Eq. (2) and for the GB model from

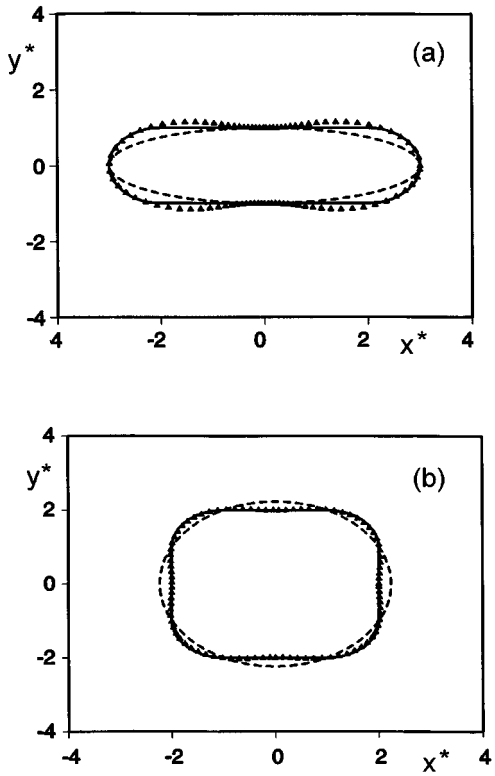

FIG. 1. Comparison of the scaled range parameter $\sigma^*(\equiv\sigma(\hat{u}_1,\hat{u}_2,\hat{r})/\sigma_0)=\sqrt{x^{*2}+y^{*2}}$, and the shape of the excluded volume for the three models: hard oblate spherocylinder (solid line), our model via Eq. (2) (triangles), and GB via Eq. (4) (dashed line). (a) Parallel configurations: $\alpha_1=\alpha_2=0$, $\theta=\beta_1=\beta_2=90°$, and φ is varied. (b) Perpendicular configurations: $\alpha_1=\alpha_2=\beta_2=0°$, $\theta=\beta_1=90°$, and φ is varied.

$$\sigma(\hat{u}_1,\hat{u}_2,\hat{r})=\sigma_0\left[1-\frac{\chi}{2}\left(\frac{(f_1+f_2)^2}{1+\chi f_0}+\frac{(f_1-f_2)^2}{1-\chi f_0}\right)\right]^{-1/2}, \quad (4)$$

where $\chi=(\kappa^2-1)/(\kappa^2+1)$ is determined by the shape anisotropy of the ellipsoid, κ, defined as $\kappa=\sigma_f/\sigma_e$. The parameters σ_e and σ_f reflect the diameter and breadth of the ellipsoidal particles. σ_e and σ_f are defined as the separations at which the attractive and repulsive terms in the potential cancel when the particles are in the edge-to-edge and face-

TABLE II. Expansion coefficients for the potential range and strength parameters. An oblate spherocylinder with shape anisotropy $(D+L)/L=3$ was taken as a reference to determine the expansion coefficients for range parameter via Eq. (2). The coefficients for the potential well depth parameter were determined via Eq. (5) by mapping onto the GB strength parameter with $\epsilon_e/\epsilon_f=\frac{1}{5}$ and $\sigma_f/\sigma_e=\frac{1}{3}$, and (I) $\mu=2$, $\nu=1$ and (II) $\mu=1$, $\nu=2$.

	σ_{000}	σ_{cc2}	σ_{220}	σ_{222}	σ_{224}
	2.34	−1.52	−0.64	−0.69	1.97
	ϵ_{000}	ϵ_{cc2}	ϵ_{220}	ϵ_{222}	ϵ_{224}
I	2.24	3.58	3.16	4.29	1.30
II	3.12	5.85	7.50	9.06	0.06

to-face configurations, respectively. In Fig. 1(a) we show a comparison of the range parameter, and the shape of the excluded volume for parallel configurations of a pair of molecules where $\alpha_1=\alpha_2=0$, $\theta=\beta_1=\beta_2=90°$, and φ is varied. The excluded volume for these configurations reflect the shape of the molecules involved in the interaction: this is an oblate spherocylinder for our model (triangles) and hard oblate spherocylinder (solid line), and an oblate ellipsoid for the GB mode 1 (dashed line). Figure 1(b) shows a comparison of the range parameter and the shape of the excluded volume for perpendicular configurations where $\alpha_1=\alpha_2=\beta_2=0°$, $\theta=\beta_1=90°$, and φ is varied. Our model (triangles) and oblate spherocylinder (solid line) gave a rounded corner square excluded volume, as expected, while the GB model gave a circular excluded volume (dashed line). In both cases the range function for oblate spherocylinders representing disklike molecules is well represented by the S-function expansion.

B. Strength function

For a pair of identical cylindrically symmetric particles, the S-function expansion for the potential strength function, $\epsilon(\hat{u}_1,\hat{u}_2,\hat{r})$, is given as

$$\epsilon(\hat{u}_1,\hat{u}_2,\hat{r})=\epsilon_0[\epsilon_{000}S_{000}+\epsilon_{cc2}(S_{202}+S_{022})+\epsilon_{220}S_{220}+\epsilon_{222}S_{222}+\epsilon_{224}S_{224}], \tag{5}$$

where ϵ_0 is the well depth corresponding to the x configuration, where $f_0=f_1=f_2=0$; it is used to scale the energy. In general the expansion coefficients in Eq. (5) can be chosen to reflect a specific interaction of interest: ϵ_{000} determines the relative strength of the orientationally averaged interaction; ϵ_{220} is the main nematic stabilizing coefficient; ϵ_{cc2} and ϵ_{222} stabilize layered and columnar ordering for disk shaped particles; and ϵ_{224} is the quadrupolar coefficient which is important if tilted phase is desired.

To facilitate comparison of our results with studies of a GB potential model for the disklike molecules with similar attractive part but different molecular geometries, we have determined the expansion coefficients for the strength function by mapping the expansion onto that of the GB potential. The GB potential strength parameter $\epsilon(\hat{u}_1,\hat{u}_2,\hat{r})$ has the form

$$\epsilon(\hat{u}_1,\hat{u}_2,\hat{r}_r)=\epsilon_0\epsilon^{\nu}(\hat{u}_1,\hat{u}_2)\epsilon'^{\mu}(\hat{u}_1,\hat{u}_2,\hat{r}), \tag{6}$$

where $\epsilon(\hat{u}_1,\hat{u}_2)=1/[1-\chi^2 f_0^2]^{1/2}$ and

$$\epsilon'(\hat{u}_1,\hat{u}_2,\hat{r})=1-\frac{\chi'}{2}\left[\frac{(f_1+f_2)^2}{1+\chi' f_0}+\frac{(f_1-f_2)^2}{1-\chi' f_0}\right].$$

The parameter $\chi'=(\kappa'^{(1/\mu)}-1)/(\kappa'^{(1/\mu)}+1)$, together with the shape anisotropy parameter $\chi=(\kappa^2-1)/(\kappa^2+1)$, determine the anisotropy in the attractive forces, where $\kappa'=\epsilon_e/\epsilon_f$, $\kappa=\sigma_f/\sigma_e$, and the subscripts e and f refer to edge-to-edge and face-to-face configurations, respectively. The GB strength parameter was parametrized to enable the likelihood of a columnar phase formation with $\kappa'=\frac{1}{5}$ and $\kappa=\frac{1}{3}$, which is the inverse of that used for most studies of prolate GB particles.

The two exponents μ and ν in the well depth function of the GB potential take different sets of values without affecting the relative well depth for the face-to-face (ϵ_f) and edge-to-edge (ϵ_e) configurations. Table III gives $\epsilon(\hat{u}_1,\hat{u}_2,\hat{r})$ for four configurations using the two common sets of the parameters μ and ν (set I: $\mu=2$, $\nu=1$; and set II: $\mu=1$, $\nu=2$). For $\mu\leqslant\nu$, the potential wells for all the configurations are deeper than those for $\mu>\nu$. This gives a wider range of stability for the translationally ordered phases (crystal, smectic, and columnar). For $\mu>\nu$, the potential wells for all the configurations are relatively shallower than those for $\mu<\nu$. This gives a narrower range of stability for the translationally ordered phases and a wider range of stability for the orientationally order phases such as the diskotic-nematic phases.

In this study we have determined the expansion coefficients of the strength parameter $\epsilon(\hat{u}_1,\hat{u}_2,\hat{r})$ for the two sets of the exponents. For each set, configurations which were considered to be important to reproduce the well depth function were identified. The well depth for a given configuration was determined from the GB model with the appropriate parameters, say ϵ_i. The more general least squares objective function χ^2_ϵ was defined as

$$\chi^2_\epsilon=\sum_{i=1}^{N} w_i[\epsilon_i-\epsilon(\hat{u}_1,\hat{u}_2,\hat{r})]^2, \tag{7}$$

where $\epsilon(\hat{u}_1,\hat{u}_2,\hat{r})$ is given by Eq. (5), N is the number of configurations identified, and w_i is a weighting function for the ith configuration adjusted to give the best fit. The expansion coefficients in Eq. (5) were determined as those which minimized χ^2_ϵ over 33 configurations. The well depth function is a completely different function from the range function. The configurations of importance are different for the two functions. Consequently a different set of weighting functions was needed to fit the strength parameter. The well depths for the four main configurations, end to end (e) and face to face (f) with parallel configurations, edge to edge with perpendicular configuration (x), and face to edge (T), are fitted with an absolute error of 0.003. The overall comparison is given in Fig. 2. The expansion coefficients are summarized in Table II. Positive values of ϵ_{cc2} and ϵ_{222} favor face-to-face configurations which stabilize a columnar phase. Positive values of ϵ_{224}, the quadrupolar coefficient, and ϵ_{220} favor a parallel configuration of molecules stabilizing the diskotic-nematic phase. Comparison of the two sets of coefficients show that set II should show a stronger columnar order stabilizing effect and a weaker diskotic-nematic stabilizing effect. This suggests a wider columnar range of stability, and a narrower range of diskotic-nematic stability. Parameter set I is predicted to show a wide range of diskotic-nematic range of stability. This expansion of the strength parameter can be parametrized to simulate molecules which would ''prefer'' to orient themselves at an angle with respect to the column to form tilted phases.

In Fig. 2(a) we show a comparison of the well depth for configurations where $\alpha_1=\alpha_2=\beta_1=\beta_2=\phi=0°$, and θ is varied, where the configuration changes from face to face to edge to edge. The solid line represents predictions of the GB model, and the dashed line shows predictions of our model obtained via Eq. (5). Figure 2(b) shows the case for configu-

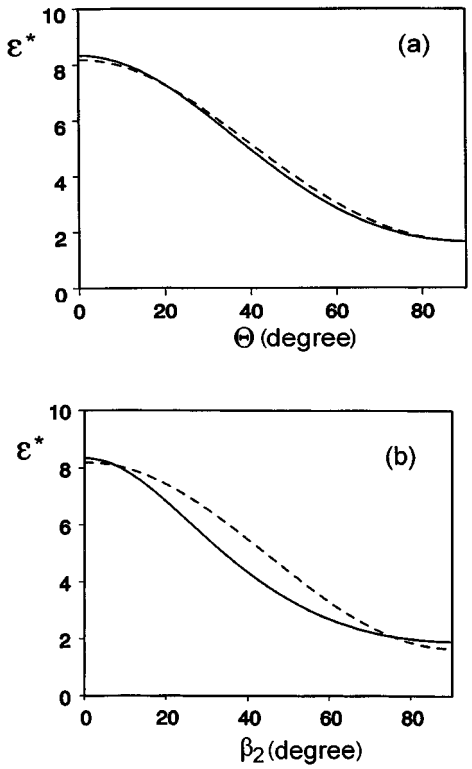

FIG. 2. Comparison of the scaled strength parameter $\epsilon^* = \epsilon(\hat{u}_1, \hat{u}_2, \hat{r})/\epsilon_0$, obtained from our model via Eq. (5) (dashed line), and GB via Eq. (6) (solid line). (a) $\alpha_1 = \alpha_2 = \beta_1 = \beta_2 = \phi = 0°$, and θ varied. (b) $\alpha_1 = \alpha_2 = \phi = 0°$, $\beta_1 = \theta = 0°$, and β_2 varied.

rations where $\alpha_1 = \alpha_2 = \phi = 0°$, $\beta_1 = \theta = 90°$, and β_2 is varied. In both of these special cases the well depth is well represented.

III. DETAILS OF THE SIMULATION

To explore the value of the model potential we have proposed for the studies of diskotic-liquid crystals, we carried out detailed simulation. A Monte Carlo algorithm with periodic boundary conditions was used, which allowed the box shape to fluctuate between the initial tetragonal shape and a cubic shape while keeping the box volume and its temperature constant [27]. This algorithm has the advantage of facilitating the equilibration process by allowing the system to come out of quasiequilibrium states. Allowing changes in the shape of the sample box allows changes in the phases to occur more easily. Restricting the shape of the box to fluctuate between the initial tetragonal shape and a cubic shape would prevent formation of structures stabilized by the box shape, and would allow the system to determine its equilibrium box shape. A detailed study was made on a system of 512 particles with a packing fraction (Nv_0/V) equal to 0.55, where $v_0 = (\Pi L^3/8)[2(D/L)^2 + \Pi(D/L)]$ is the volume of a molecule which is defined as the volume of an oblate spherocylinder with shape anisotropy $(D+L)/L$ equal to 3, V is the volume of the sample box and $L = \sigma_f (\equiv \sigma_0)$.

TABLE III. A comparison of the well depths of the GB model for two sets of exponents. The anisotropies in the shape and attractive force are chosen to be $\kappa (\equiv \sigma_f/\sigma_e) = \frac{1}{3}$ and $\kappa' (\equiv \epsilon_e/\epsilon_f) = \frac{1}{5}$ to reflect oblate ellipsoidal symmetry. (I) $\mu = 2$, $\nu = 1$. (II) $\mu = 1$, $\nu = 2$.

	Face to face ϵ_f/ϵ_0	Edge to edge ϵ_e/ϵ_0	T shaped ϵ_τ/ϵ_0	Cross shaped ϵ_x/ϵ_0
I	25/3	5/3	$(15-5\sqrt{5})/2$	1
II	125/9	25/9	5/3	1

The simulation was started by arranging the particles on a fcc lattice where the x and y directions are stretched by a factor of σ_e/σ_f reflecting the shape anisotropy of the particles. The lattice was chosen to have 4, 4, and 8 unit cells along the x, y, and z directions to match the number of lattice sites with the number of particles. This choice gave the tetragonal box an almost cubic shape with a reasonable number of particles along the three directions to ensure that the box dimensions were larger than the potential cutoff distance in all three orthogonal directions. The initial dimensions of the box were determined by the dimensions of the starting fcc lattice and the volume of the system. The instantaneous dimensions of the box were used to reduce the corresponding components of coordinates of the particles. This restricted each component of a particle in a reduced coordinate to vary between zero and unity. This reduction of particle components of the coordinate with the corresponding box length enabled us to perform Monte Carlo moves separately on the tetragonal box shape and the position of particles. A change in the tetragonal box shape was achieved by changing the dimensions of the box keeping its volume constant. During the simulation the box dimensions were allowed to fluctuate within a maximum of $2\sigma_0$ from the initial dimension to allow the system to fluctuate about a cubic box shape.

In this simulation we have performed the three Monte Carlo moves separately—change of box shape, change of translational position, and change of orientational position of the molecules—to increase the rate of equilibration and the efficiency of the sampling. The maximum allowed changes, say Δ_b, Δ_t, and Δ_r, corresponding to changes in dimensions of the box, the translational coordinate components, and the orientations about a randomly chosen axis, respectively, were adjusted every macrocycle so that the acceptance ratio was in the range 0.4–0.6. A macrocycle was typically 2000 cycles, and a cycle typically consisted of 512 attempted orientational moves followed by 512 attempted translational moves and one or two attempted box dimension changes. Trial orientational moves were generated following the Barker-Watts technique, in which a particle was rotated by a random amount about a laboratory axis selected at random [28]. Translational moves were generated by sequentially choosing a particle and displacing it by $\Delta_t \xi_t$ in reduced units along a randomly chosen axis, where ξ_t is a random number between -0.5 and 0.5. The coordinates of the interacting particles were then converted to scaled units to calculate the change in configurational energy. A change in box dimension was attempted by randomly choosing a laboratory axis; a random number between -0.5 and 0.5 was then generated, say ξ_b. A multiplying factor was calculated as $\exp(\Delta_b \xi_b)$ for the box dimension along the randomly chosen axis, and the corresponding ones for the other two, to leave

the tetragonal box volume constant. The old and new sets of box dimensions were used to convert the reduced coordinates of particles to the corresponding sets of scaled coordinates. The change in configurational energy as a result of the attempted change in the box shape was then calculated. The attempted change in box shape, as well as translational and rotational moves, were accepted following the standard Metropolis algorithm [29,30].

The last configuration of each production stage was used as the starting configuration for the next temperature. Equilibration was monitored via the internal energy and orientational order parameters subaveraged over a macrocycle. Typically 20 macrocyles were generated to equilibrate the system. The structural and thermodynamic properties were calculated from a minimum of 40×10^6 configurations. Near the temperatures where we expected a phase transition to occur, we performed longer runs. To reduce the computational time a spherical cutoff of $4\sigma_0$ with a Verlet neighbor list [31] was employed; this list was extended up to $4.5\sigma_0$ and updated every 20 cycles. The statistical errors in the final values of properties were estimated from 20 successive subaverages of the properties each calculated over a macrocycle configurations.

The detection of different kinds of orientational and translational orders in a computer simulation requires the determination of the appropriate radial distribution functions and order parameters. In order to study the translational order in the system, we calculated the orientationally averaged radial distribution function, $g(r^*)$, which gives the probability of finding a molecule at a distance r^* from the one at the origin, relative to the probability expected for a completely random distribution at the same density. It is conveniently defined for evaluation by computer simulation as [15,30]

$$g(r^*)=\frac{1}{4\pi N\rho r^{*2}}\left\langle \sum_i \sum_{j\neq i} \delta(r^*-r^*_{ij})\right\rangle, \tag{8}$$

where $r^*=r/\sigma_0$. $g(r^*)$ enables us to characterize at least the crystalline and translationally disordered phases. However, this alone is insufficient to distinguish between the different kinds of mesophase ordering. Hence other functions that probe the translational ordering of the molecules in orientationally ordered phases must be introduced. In particular we have calculated the distribution function parallel to the director $g_{\parallel}(r^*_{\parallel})$ which is sensitive to the arrangement of molecules in layers and the distribution function $g_c(r^*_c)$ which is sensitive to the regular stacking of molecules in columns. These structural properties are defined as [15,30]

$$g_{\parallel}(r^*_{\parallel})=\frac{1}{l^*_x l^*_y N\rho}\left\langle \sum_i \sum_{j\neq i} \delta(r^*_{\parallel}-\hat{n}\cdot\mathbf{r}^*_{ij})\right\rangle \tag{9}$$

and

$$g_C(r^*_C)=\frac{4}{\pi[(D+L)/2L]^2 N\rho}\left\langle \sum_i \sum_{j\neq i} \Delta_{ij}\delta(r^*_C-\hat{u}_i\cdot\mathbf{r})\right\rangle, \tag{10}$$

where Δ_{ij} is equal to unity if $|\hat{u}_i\cdot\mathbf{r}^*_{ij}|^2+[(D+L)/2L]^2 > |r^*_{ij}|^2$, and zero otherwise; these are convenient for evaluation by computer simulation. l^*_x and l^*_y are the average reduced box dimensions along x and y axes. The degree of order within a layer is monitored via the radial distribution function perpendicular to the director $g_{\perp}(r^*_{\perp})$, defined as [15,30]

$$g_{\perp}(r^*_{\perp})=\frac{1}{2\pi l^*_t N\rho r^*}\left\langle \sum_i \sum_{j\neq i} \delta(r^*_{\perp}-r^*_{ij,\perp})\right\rangle, \tag{11}$$

where $|\hat{n}\cdot\mathbf{r}^*_{ij}|<l^*_t/2$, $l^*_t=2$ is a slice thickness about the particle considered, and $r^*_{ij,\perp}=(|r^*_{ij}|^2-|n\cdot r^*_{ij,\perp}|^2)^{1/2}$. For all the distribution functions δ is a Dirac delta function replaced by unity in a small range of separation taken to be 0.01 in reduced units, and a histogram was compiled of all pair separations falling within each such range.

The hexagonal arrangement of columns of molecules and molecules within a layer was monitored by calculating the bond order parameter defined as

$$\Psi_6=\left|\left\langle \frac{1}{N}\sum_j \frac{1}{n^j_b}\sum_{\langle kl\rangle} w_{kl}\exp(6i\theta_{kl})\right\rangle\right|, \tag{12}$$

where n^j_b is the number of pairs of nearest neighbors of the jth molecule, $\langle kl\rangle$ implies a sum over all possible pairs of neighbors, and θ_{kl} is the angle between the unit vectors along the projections of the intermolecular vectors between molecule j and its neighbors k and l onto a plane perpendicular to the director. $w_{kl}=1$ if $\mathbf{r}^*_{jk}$ and $\mathbf{r}^*_{jl}$ lie within a cylinder of diameter 3.5 and thickness 2 centered at particle j, and zero otherwise. This range was chosen such that only molecules in the first coordination shell contribute to the sum. Ψ_6 takes unity for a phase with a perfect hexagonal bond order, zero for the isotropic phase, and an intermediate value for a phase with intermediate bond order.

Calculations of two of the radial distribution functions $g_{\parallel}(r^*_{\parallel})$ and $g_{\perp}(r^*_{\perp})$ and the bond order parameter require knowledge of the director orientation $\hat{n}$. In computer simulation the director is not known *a priori*, and it fluctuates during the evolution of the system. In general the second-rank orientational order parameter and the direction of the director for a given configuration can be calculated from a second-rank tensor defined as [11,32]

$$Q_{\alpha\beta}=\frac{1}{N}\sum (3u^i_\alpha u^i_\beta-\delta_{\alpha\beta})/2, \tag{13}$$

where u^i_α, and $\alpha=x, y, z$ is the direction cosine of the unit vector describing the orientation of the ith molecule with respect to an arbitrary space-fixed frame. In the phases where the configurations show considerable orientational order, the fluctuation of the director orientation during a cycle is insignificant. Considering this we were able to reduce the computational time by sampling the Q tensor only once at the end of a cycle and accumulating it for 30–50 configurations. The averaged Q tensor was then diagonalized once at the end of every 30–50 cycles. Its largest positive eigenvalue was then accumulated and at the end of the run averaged to give the second-rank order parameter, $\overline{P_2}$. Whenever a director orientation was needed to calculate the other structural properties the eigenvectors of the last averaged Q tensor were determined and the one associated with the largest eigenvalue

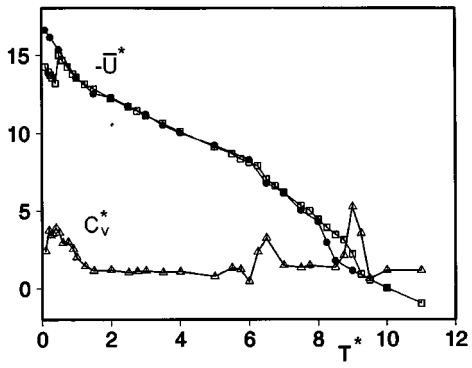

FIG. 3. The scaled internal energy $\overline{U^*}(\equiv\langle U/N\epsilon_0\rangle)$ (□) and heat capacity $C_V^*(\equiv C_V/Nk)$ (△) as a function of the scaled temperature $T^*(\equiv kT/\epsilon_0)$ for model I obtained from the heating run. The internal energy results obtained from the cooling run starting from the isotropic phase are indicated as (●). Lines are drawn through the points as a guide to the eye.

was identified with the director. Once the director orientation is located, a variety of structural properties can be calculated for a given configuration. The frequency of eigenvector determination depends on the frequency of sampling of structural properties which depend on the orientation of the director.

IV. SIMULATION RESULTS AND DISCUSSION

We have simulated two parametrizations of the model potential. The two sets of the expansion coefficients for the strength parameter are given in Table II. For convenience we shall call the model potential with the first set of coefficients model I, and that with the second set model II. A detailed simulation study was carried out at a packing fraction of 0.55. We shall first present and discuss the simulation results for model I, and then those for model II. Whenever possible we shall give a comparison of the results for the two models, and also compare those with the results obtained for the GB model of oblate ellipsoids.

Figure 3 shows the variation of the scaled internal energy $U^*(\equiv\langle U/N\epsilon_0\rangle)$ and heat capacity $C_V^*(\equiv C_V/Nk)$ as a function of the scaled temperature $T^*(\equiv kT/\epsilon_0)$ for model I. The error bars estimated for U^* from 20 block averages were found to be less than the experimental points. The internal energy for the heating run is represented by open squares, and that for the cooling run by filled circles. The internal energies for the heating and cooling runs show a difference at low temperatures. This shows that the low temperature equilibrium crystal structure is not fcc. At absolute zero the equilibrium crystal structure is hexagonally close packed (hcp) layers stacked in an *AAA* structure. The fcc structure appears to be mechanically stable and thermodynamically unstable. A fcc structure was chosen as the starting crystal structure to enable us to easily identify the diskotic-columnar phase as the equilibrium structure when it is self-organized on melting of the crystal. The heat capacity shown in Fig. 3 was determined by numerically differentiating the internal energy obtained from the heating run fitted to a smoothing cubic spline function. The positions of the three heat capacity peaks suggest the existence of four regions of stable phases with transition temperatures T^* of 0.45, 6.75, and 9.00. The melting transition appears rather unusual, as it occurs with a reduction in entropy (that is, $\Delta S/Nk$ is -1.58), which suggests that the fcc structure is not the equilibrium crystal structure. The melting transition was studied for two other packing fractions of 0.45 and 0.66. In all three cases the fcc melted into a hexagonal columnar phase. At absolute zero the equilibrium crystal structure is *AAA*-stacked hcp layers. It is easier for the system to go to the equilibrium hcp structure on cooling from the high temperature columnar phase, than from the fcc structure which is mechanically stable at low temperatures. The two heat capacity peaks around the scaled temperatures of 6.75 and 9.00 are associated with weak first order transitions. For these the transitional entropies $\Delta S/Nk$ are estimated to be 0.11 and 0.15, respectively. Based on the behavior of real diskotic liquid crystals, it seems reasonable to identify the four phases as crystal, diskotic columnar, diskotic nematic, and isotropic, appearing in succession with increasing temperature. Heat capacity peaks alone are not sufficient to identify positions of phase transitions. In the following we shall present the structural properties and snapshots of configurations representing the various phases, to demonstrate the sequence of phase transitions exhibited by our model potential.

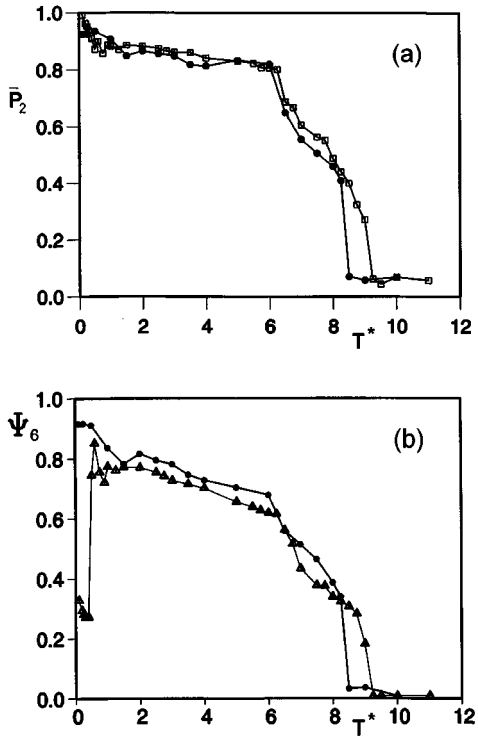

FIG. 4. Plots of order parameters as a function of scaled temperature for model I. The points are connected by lines to serve as a guide to the eye. (a) Second rank orientational order parameter P_2 (□, heating; ●, cooling). (b) Bond order parameter Ψ_6 (△, heating; ●, cooling).

In Fig. 4(a) we present the temperature dependence of the second-rank orientational order parameter P_2. Open squares represent the heating run, and filled circles the cooling run. In agreement with the predictions based on the heat capacity peaks, four stable regions can be identified from this plot. In

the crystal phase the orientational order parameter shows a strong temperature dependence; it changes smoothly from the crystal phase to the columnar phase. Both phases are highly orientationally ordered. Over the entire region of the columnar phase, $\overline{P_2}$ shows a relatively weak temperature dependence; it shows a discontinuous reduction across the columnar to diskotic-nematic transition and a strong temperature dependence in the diskotic-nematic phase. It remains small but finite in the isotropic phase. Such behavior usually arises due to the method of determining the order parameter and the small number of particles studied. Indeed, in the isotropic phase $\overline{P_2}$ is predicted to show a size dependence of the order of $1/\sqrt{N}$ [11]. The error bars estimated for $\overline{P_2}$ from 20 block averages were found to be less than the experimental points.

In Fig. 4(b) we present the temperature dependence of the bond order parameter Ψ_6. The triangles are for the heating run and filled circles are for the cooling run. The bond order parameter for the heating and cooling runs show a large difference at low temperatures. The heating run was started from the fcc structure. For a perfectly ordered fcc structure Ψ_6 is 0.33. On melting of the fcc structure, the system self-organized into hexagonally packed columns which have a large value for the bond order parameter. For a perfectly ordered hexagonally packed column, Ψ_6 takes its maximum value of unity. On cooling the diskotic-columnar phase to low temperatures the system goes into its equilibrium structure of *AAA*-stacked hcp layers, which gives a high value for Ψ_6. The plot of the bond order parameter as a function of temperature shows the four regions and the location of the transitions quite clearly and are consistent with those predicted based on the plots of C_V^* and $\overline{P_2}$. In the fcc phase, Ψ_6 shows a strong temperature dependence. At the fcc-columnar phase transition the bond order parameter increases drastically from about 0.25 to 0.8, indicating the melting of the fcc phase and the formation of a hexagonally arranged phase. Over the entire region of the diskotic-columnar phase the bond order parameter shows a weak temperature dependence. Ψ_6 shows a discontinuity across the columnar to a diskotic-nematic transition. It varies from 0.4 to 0.3 in the diskotic-nematic phase. This reflects the extent of the local short-range translational order in the nematic phase. In the isotropic phase the bond order parameter vanishes. The error bars estimated for Ψ_6 over 20 block averages were found to be less than the experimental points.

Visual inspection of typical configurations complements the predictions based on thermodynamic and structural properties calculated for the various phases. In Fig. 5 we show snapshots of the last configurations taken from the production stages from simulations at five selected temperatures. These are viewed at an angle from the director chosen to show some aspects of the structure of the corresponding systems. The views along the director are shown in Fig. 6. The particles are represented as disklike objects and, for the sake of clarity, the dimensions of the particles are reduced by about 20%.

Figures 5(a) and 6(a) show snapshots at a scaled temperature of 0.4, which is just before the fcc crystal melts. Figure 5(a) shows a layer by layer arrangement of particles, and Fig. 6(a) shows the rectangular arrangement of particles within a layer which is typical of a fcc structure. These pictures alone are not sufficient to characterize the structure of the phase. In Fig. 7(a) we give the pair distribution functions $g(r^*)$ and $g_\perp(r_\perp^*)$ calculated via Eqs. (8) and (11), respectively. The

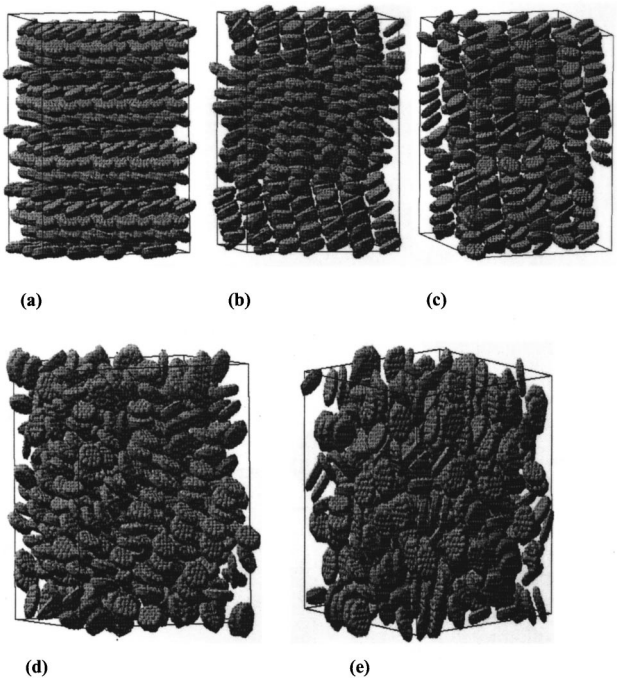

FIG. 5. Snapshots of final configurations for model I taken from the production stages at five reduced temperatures as viewed at an angle with respect to the director. For the sake of clarity the dimensions of the particles are scaled down by 20%. (a) 0.40 (fcc). (b) 0.5 (D_{ho}). (c) 6.0 (D_{hd}). (d) 8.0 (N_D). (e) 10.00 (isotropic).

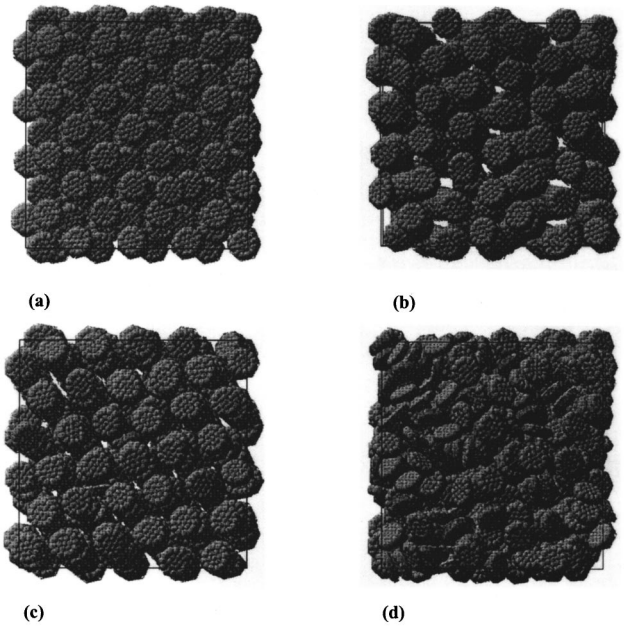

FIG. 6. Snapshots of the final configurations for model I taken from the production stage at four scaled temperatures as viewed along the director. For the sake of clarity the dimensions of the particles are reduced by 20%. (a) 0.40 (fcc), (b) 0.5 (D_{ho}). (c) 6.0 (D_{hd}). (d) 8.0 (N_D).

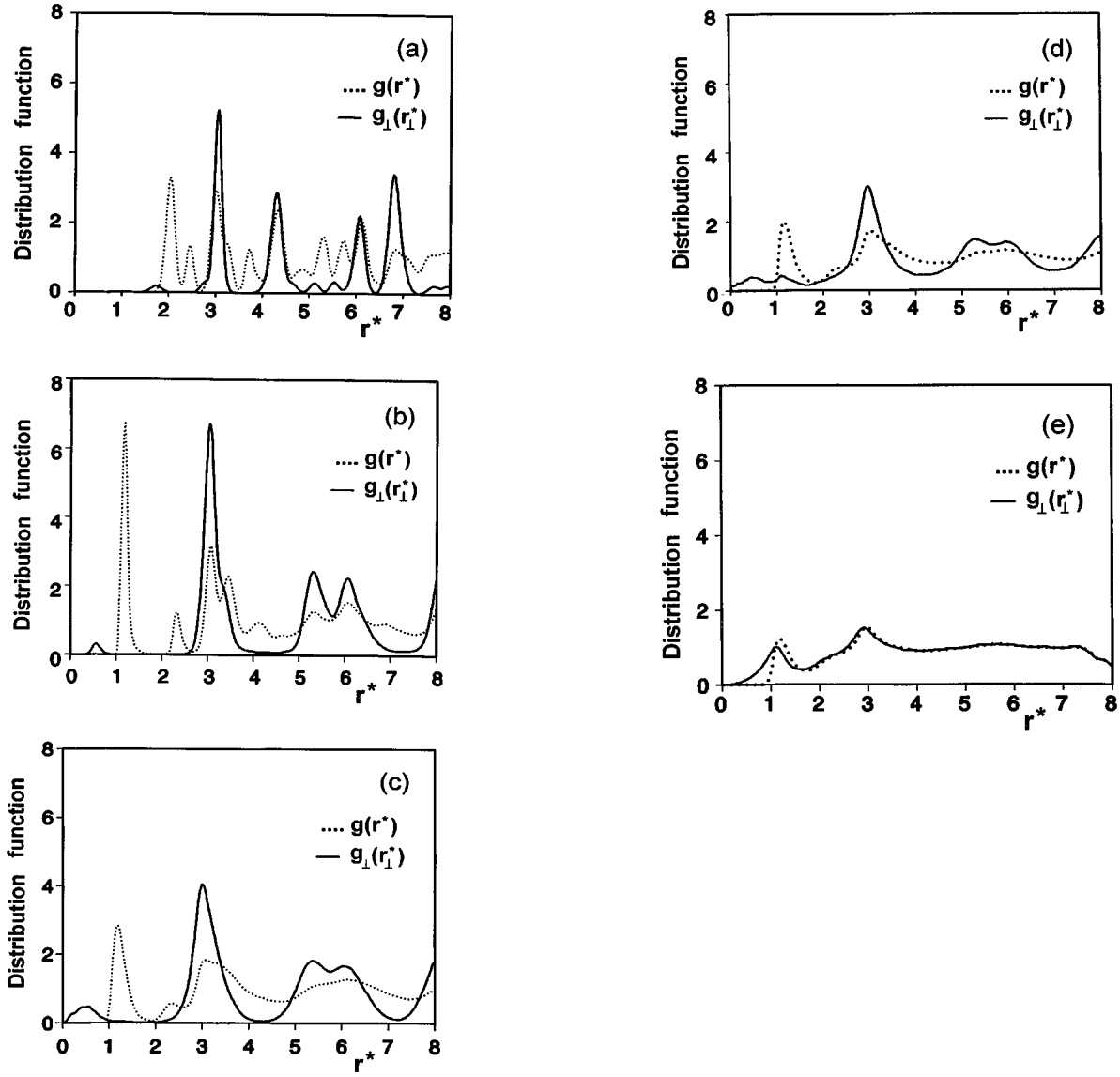

FIG. 7. Plots of pair distribution functions for model I: $g(r^*)$ (dotted line) obtained via Eq. (8) and $g_\perp(r_\perp^*)$ (solid line) obtained via Eq. (11) for five reduced temperatures. (a) 0.40 (fcc). (b) 0.5 ($D_{\rm ho}$). (c) 6.0 ($D_{\rm hd}$). (d) 8.0 (N_D). (e) 10.00 (isotropic).

four main peak positions of $g(r^*)$ for a perfect fcc structure are at reduced separations of approximately 2, 3.16, 4.24, and 6, while the first four peak positions of $g_\perp(r_\perp^*)$ correspond to reduced separations of about 3.16, 4.24, 6, and 6.78. The relative peak heights of the first three peaks is 2:1:1. The main peak positions in Fig. 7(a) match those of the expected peak positions for a perfect fcc structure. The plots of $g_c(r_c^*)$ and $g_\parallel(r_\parallel^*)$, obtained via Eqs. (9) and (10), respectively, are shown in Fig. 8(a). The main features of these plots are that the peaks for $g_\parallel(r_\parallel^*)$ are of uniform height and are uniformly spaced with an average spacing of about 1.1 scaled units, while those for $g_c(r_c^*)$ are also of uniform peak heights but with twice the peak spacings for $g_\parallel(r_\parallel^*)$. However, $g_c(r_c^*)$ has already started showing small secondary peaks at some of the intermediate positions indicating imperfections in the lattice structure. The structure of these four pair distribution functions, together with the density distributions along the three arbitrary laboratory axes, which are all found to be periodic, characterize this phase as the starting fcc crystal.

The stable structure over the wide temperature range of 0.45 to 6.75 is characterized as a hexagonal columnar phase. Figure 5(b) shows a snapshot of a configuration at a temperature of 0.5. This is just after melting, and the molecules are stacked in columns which have a parallel arrangement on a local scale. Figure 6(b) shows a snapshot of the same configuration but now viewed parallel to the director. This shows that the columns are arranged on a two-dimensional hexagonal lattice. In Fig. 7(b) we present the radial distribution functions $g(r^*)$ and $g_\perp(r_\perp^*)$. The main features of $g(r^*)$ are the principal peaks around 1.1 for the face-to-face stacking, around 3.3 for the edge-to-edge arrangement, and a doublet between 5 and 7 for a hexagonal arrangement. This interpretation is consistent with the form of $g_\perp(r_\perp^*)$: a principal peak around 3.2 and a doublet between 5 and 7. A doublet in these pair distribution functions is usually taken as the signature of a hexagonal arrangement of molecules. However, such doublets in these distribution functions are also consistent with other molecular organizations, for ex-

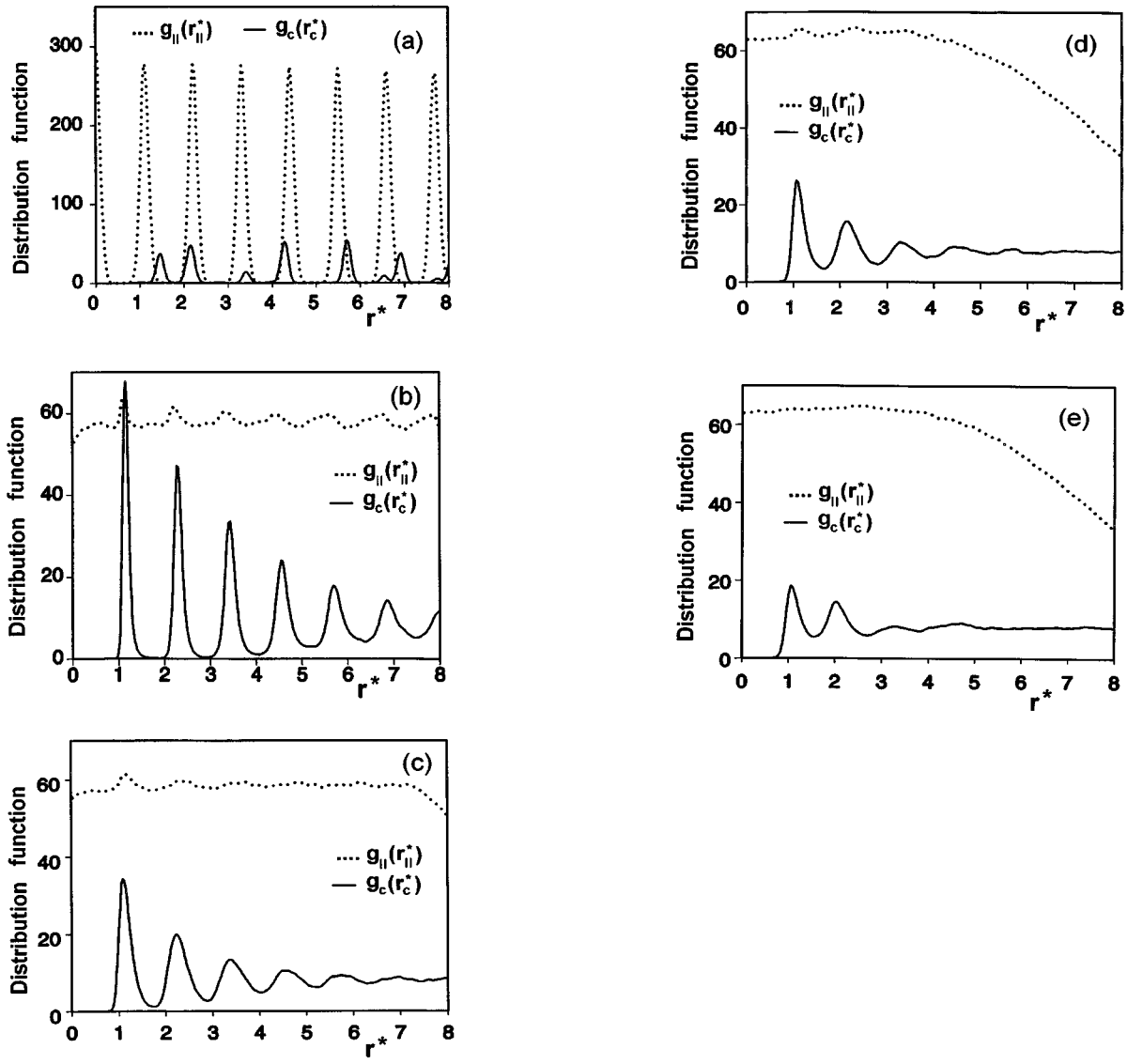

FIG. 8. Plots of pair distribution functions for model I: $g_{\|}(r^*_{\|})$ (dotted line) obtained via Eq. (9) and $g_c(r^*_c)$ (solid line) obtained via Eq. (10) for five reduced temperatures. (a) 0.40 (fcc), (b) 0.5 (D_{ho}). (c) 6.0 (D_{hd}). (d) 8.0 (N_D). (e) 10.00 (isotropic).

ample hcp crystal and hexatic smectic-B phases. In Fig. 8(b) we give $g_{\|}(r^*_{\|})$ and $g_c(r^*_c)$. At a low temperature such as 0.5, the system has a weak layered structure with strongly correlated stacking of molecules in columns. The peaks in $g_{\|}(r^*_{\|})$ and $g_c(r^*_c)$ are regularly spaced, with an average scaled spacing of 1.1. The peak heights in $g_c(r^*_c)$ show an exponential decay as a function of molecular separations of the form $Ae^{-r_c/\xi}$, where A is 1.55 and the correlation length ξ is 3.89. Hexagonally arranged columns of regularly stacked disks is a characteristic behavior of a D_{ho} phase. In Figs. 5(c) and 6(c) we show snapshots of configurations at a temperature of 6.0, just before the columnar phase undergoes transition to the diskotic-nematic phase. The molecules are stacked in parallel columns which are arranged on a two-dimensional hexagonal lattice. The pair distribution functions $g(r^*)$ and $g_{\perp}(r^*_{\perp})$ are presented in Fig. 7(c); here the peaks are broadened, although they show similar features to those at a reduced temperature of 0.5. Significant changes in the molecular stacking within a column is reflected in $g_{\|}(r^*_{\|})$ and $g_c(r^*_c)$, and $g_{\|}(r^*_{\|})$ shows no structure. The correlation between positions of molecules within a column appears to vanish within five molecular thicknesses. The structure of these four pair distributions are similar to those in the nematic phase shown in Figs. 7(d) and 8(d), indicating uniform liquidlike mass distribution. The stacking of molecules in long hexagonally arranged columns with liquidlike structure within columns is defined as a D_{hd} phase.

The diskotic-nematic phase is found to be stable over the scaled temperature range of 6.75–9.0. Snapshots of the last configuration for the production stage at a scaled temperature of 8.0 viewed from an angle to the director is shown in Fig. 5(d). A view parallel to the director is given in Fig. 6(d). The system appears to have a few molecules stacked in short columns. This is evident from the pair distribution function of $g_{\|}(r^*_{\|})$ shown in Figs. 7(d) and 8(d). The four pair distribution functions in the columnar phase (D_{hd}) at $T^*=6.0$ and the diskotic-nematic phase at $T^*=8.0$ appear to show similar features. The two phases are clearly distinguished with the

help of the configurational snapshots shown in Figs. 5(c) and 5(d). The nematic order parameter varies from 0.6 to 0.27. At $T^*=9.0$ the system undergoes a weak first order phase transition to an isotropic phase.

In Fig. 5(e) we show a snapshot of the last configuration taken from the production stage at T^* equal to 10.00. At this temperature the system is characterized as isotropic. However, due to finite size effects and also due to the method by which the order parameter is calculated the system shows a small finite orientational order parameter. Although the director associated with the instantaneous order parameter fluctuates quite significantly, it is still of interest to calculate $g_\perp(r_\perp^*)$ and $g_\parallel(r_\parallel^*)$. The pair distribution functions $g_\parallel(r_\parallel^*)$ and $g_c(r_c^*)$ are presented in Fig. 8(e), and $g_\parallel(r_\parallel^*)$ indicates a uniform mass distribution along the director, whereas $g_c(r_c^*)$ clearly shows two peaks indicating the short-range stacking of molecules. This is important evidence that the pair potential favors the formation of a columnar order. $g(r^*)$ and $g_\perp(r_\perp^*)$, presented in Fig. 7(e), show peaks around 1 and 3. Such structures for these distribution functions are unusual. A similar structure was predicted for dipolar hard oblate ellipsoids at sufficiently high dipolar strength [33]. The first peak corresponds to the face-to-face arrangement of two molecules, and the second peak has contributions from the edge-to-edge arrangement of two molecules and face-to-face arrangement of three molecules. These peaks reflect the shape anisotropy of the constituent molecules. The pair distribution function $g(r^*)$ obtained from molecular dynamics simulation of hard oblate spherocylinders [9], hard oblate ellipsoids [34], and GB oblate ellipsoids [17] do not appear to show the first peak.

An important distinction between the diskotic-nematic and isotropic phases is shown in the $g_\perp(r_\perp^*)$ plots presented in Figs. 7(d) and 7(e). The first peak, which is due to molecules arranged face to face and perpendicular to the director, is absent in the nematic phase. This could be taken as evidence of the lack of long-range orientational order in the isotropic phase which is responsible for the strong fluctuation of the director.

In order to make a direct comparison with the simulation of oblate ellipsoids at the same packing fraction of 0.55 and similar strength parameter, we shall next present results obtained by using potential model II. Figure 9 shows the results for the scaled internal energy $U^*(\equiv\langle U/N\epsilon_0\rangle)$ and heat capacity $C_V^*(\equiv C_V/Nk)$ determined by numerical differentiation of the internal energy as a function of the scaled temperature $T^*(\equiv kT/\epsilon_0)$. The error bars estimated for U^* over 20 block averages were found to be less than the experimental points. The two heat capacity peaks at scaled temperatures of 1.25 and 13.25 suggest the existence of three stable phases. These phases have been characterized with the help of the order parameters shown in Fig. 10. The phase sequence is established to be crystal, hexagonal diskotic columnar, and isotropic. The diskotic-nematic phase appears to be removed by this change of parameter in favor of the diskotic-columnar phase. If a diskotic-nematic phase is stable for this system, it must be over a very narrow temperature range which is difficult to determine with the current wide temperature intervals studied. Figure 11 gives snapshots of the last configurations from the production

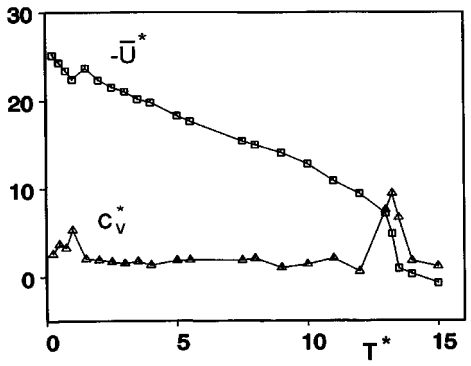

FIG. 9. The scaled internal energy $\overline{U^*}(\equiv\langle U/N\epsilon_0\rangle)$ (□) and heat capacity $C_V^*(\equiv C_V/Nk)$ (△) as a function of scaled temperature $T^*(\equiv kT/\epsilon_0)$ for model II.

stage at $T^*=1.5$, which is just after the system melts, and at $T^*=13.00$ just before the columnar phase undergoes a transition to the isotropic phase. The nature of the columnar order at these two temperatures is qualitatively and quantitatively different. The different nature of the columnar order are indicated by the pair distribution functions $g_\parallel(r_\parallel^*)$ and $g_c(r_c^*)$ shown in Fig. 12. The pair distribution at $T^*=1.5$ calculated parallel to the director indicates a weak layered structure. However, the peak spacing is half that expected for layers formed from disks of the dimensions used in this simulation. Moreover, these observations reveal that the disks within one column are staggered with respect to those in an adjacent one. The peak heights in $g_c(r_c^*)$ show an exponential decay as a function of molecular separations of the form $Ae^{-r_c/\xi}$, where $A=1.52$ and $\xi=5.32$. The bond order parameter together with the doublets in the peaks for $g_\parallel(r_\parallel^*)$ in the range of distances 5–7 indicates the arrangement of columns on a two-dimensional hexagonal lattice. This hexagonal structure is clearly observed in the snapshot of Fig. 11(b) taken parallel to the column axes. Such phases with such characteristic intercolumnar correlations have been observed for other simulations of oblate ellipsoids [17]. In our system the intercolumnar correlation is found to be stable only at the temperature just after the melting of the crystal. This phase has been identified as $D'_{\rm ho}$ in order to distinguish it from the uncorrelated hexagonally ordered columnar

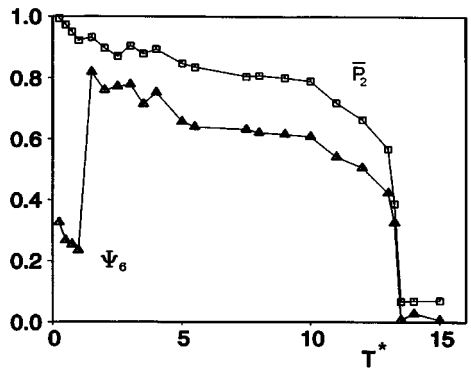

FIG. 10. Plots of the second rank orientational order parameter $\overline{P_2}$ (□), and the bond order parameter Ψ_6 (△) as a function of scaled temperature for model II.

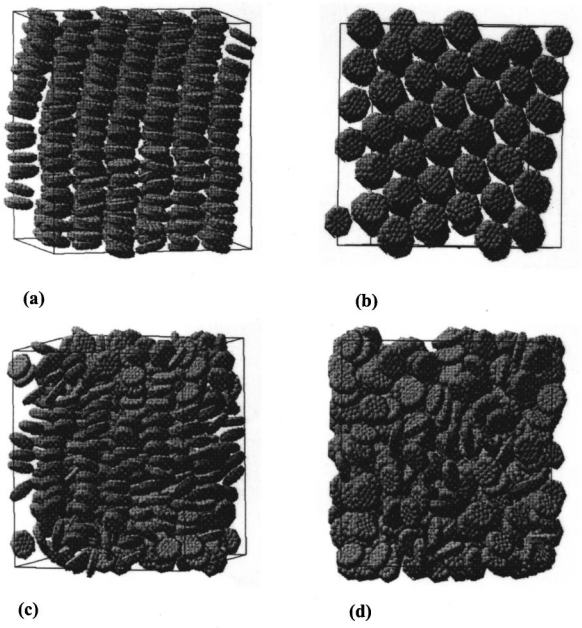

FIG. 11. Snapshots of the final configurations taken from the production stages at two scaled temperatures as viewed at angle with respect to the director [(a) and (c)] and along the director [(b) and (d)] for model II. For the sake of clarity the dimensions of the particles are reduced by 20%. (a) 1.5 (D'_{ho}, side view). (b) 1.5 (D'_{ho}, top view). (c) 13.0 (D_{hd}, side view). (d) 13.0 (D_{hd}, top view).

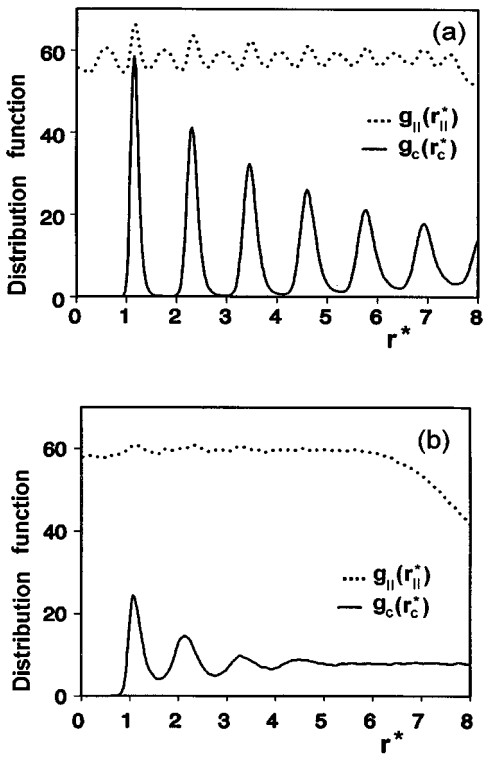

FIG. 12. Plots of pair distribution functions for model II: $g_{\parallel}(r^*_{\parallel})$ (dotted line) and $g_c(r^*_c)$ (solid line) for two reduced temperatures. (a) 1.5 (D_{ho}). (b) 13.0 (D_{hd}).

phase. The high temperature columnar phase appears to show a qualitatively different structure. The phase at a temperature close to the isotropic transition is expected to have a high degree of disorder. This is evident from the snapshots shown in Figs. 11(c) and 11(d). However, an important distinction appears in the pair distribution functions $g_{\parallel}(r^*_{\parallel})$ and $g_c(r^*_c)$ shown in Fig. 12(b). $g_{\parallel}(r^*_{\parallel})$ does not show any structure indicating the absence of any layered structure. However, $g_c(r^*_c)$ exhibits a peak structure which vanishes within four molecular thickness. These structures of the pair distribution functions together with the results on the bond order parameters and $g_{\perp}(r^*_{\perp})$ characterize the phase at $T^*=13.00$ as the D_{hd} phase.

V. CONCLUSIONS

The shifted form of Lennard-Jones 12-6 potential has proved successful in computer-simulation studies of systems composed of rodlike and disklike molecules. The range parameter $\sigma(\hat{u}_1,\hat{u}_2,\hat{r})$ for disklike molecules is estimated based on either spheres or oblate ellipsoids in the GB model. The range parameter estimated in this way appears to favor formation of the diskotic-nematic phase over the diskotic-columnar phase. The thick middle region of the ellipsoid together with its relatively tapered edge favors interdigitated packing. This makes formation of the diskotic-columnar phase difficult, and favors the diskotic-nematic phase. This effect is enhanced as the shape anisotropy decreases. We have successfully removed this problem by modeling the range parameter based on an oblate spherocylinder, which is a more realistic model to study disklike molecules. The computer simulation of our model potential clearly showed the stability of a variety of stable diskotic-columnar and diskotic-nematic phases. We have successfully demonstrated how to characterize the structure of the various diskotic phases using combinations of results obtained from the various thermodynamic and structural properties. The S-function expansion approach of the strength parameter allows each term to be associated with a specific type of interaction: isotropic, anisotropic (nematic favoring, columnar favoring, smectic favoring), and quadrupolar (responsible for tilt formation). This enables each coefficient in the expansion of the strength parameter to be fine tuned to reflect the relative strength of a specific type of interaction. S functions can be evaluated efficiently by computers. This makes our model potential computationally cheaper. This reduction in computer time could be significant when studying systems with large sample size or systems with molecules made up of units joined together to study a variety of geometries.

ACKNOWLEDGMENTS

The author acknowledges the Royal Society, the International Centre for Theoretical Physics, the British Council, and the University of Southampton for financial support; Professor G. R. Luckhurst and Professor T. J. Sluckin for their hospitality; and Addis Ababa University for the study leave.

[1] S. Chandrasekhar, B. K. Sadashiva, and K. A. Suresh, Pramana **9**, 471 (1977).
[2] D. Goldfarb, R. Poupko, Z. Luz, and H. Zimmermann, J. Chem. Phys. **79**, 4035 (1983).
[3] H. P. Hinov, Mol. Cryst. Liq. Cryst. **136**, 221 (1986).
[4] S. Chandrasekhar, in *Advances in Liquid Crystals*, edited by G. H. Brown (Academic, New York, 1982), Vol. 5, p. 47.
[5] S. Chandrasekhar, Philos. Trans. R. Soc. London, Ser. A **309**, 93 (1983).
[6] S. Chandrasekhar and G. S. Ranganath, Rep. Prog. Phys. **53**, 57 (1990).
[7] S. Chandrasekhar, Liq. Cryst. **14**, 3 (1993).
[8] P. M. Zorkii and E. V. Sakhanova, Russ. J. Phys. Chem. **66**, 147 (1992).
[9] M. Wojcik and K. E. Gubbins, Mol. Phys. **53**, 397 (1984).
[10] J. Sedlbauer, S. Lasik, and A. Malijevsky, Phys. Rev. E **49**, 3179 (1994).
[11] R. Eppenga and D. Frenkel, Mol. Phys. **52**, 1303 (1984).
[12] D. Frenkel and B. M. Mulder, Mol. Phys. **55**, 1171 (1985).
[13] B. M. Mulder and D. Frenkel, Mol. Phys. **55**, 1193 (1985).
[14] M. P. Allen, Phys. Rev. Lett. **65**, 2881 (1990).
[15] J. A. C. Veerman and D. Frenkel, Phys. Rev. A **45**, 5632 (1992).
[16] M. D. de Lucha, M. P. Neal, and C. M. Care, Liq. Cryst. **16**, 257 (1994).
[17] A. P. J. Emerson, G. R. Luckhurst, and S. G. Whatling, Mol. Phys. **82**, 113 (1994).
[18] J. L. Lebowitz and J. W. Perram, Mol. Phys. **56**, 4213 (1983).
[19] D. Frenkel, Mol. Phys. **60**, 1 (1987).
[20] H. B. Zewdie (unpublished).
[21] H. B. Zewdie, J. Chem. Phys. (to be published).
[22] J. G. Gay and B. J. Berne, J. Chem. Phys. **74**, 3316 (1981).
[23] R. Berardi, A. P. J. Emerson, and C. Zannoni, J. Chem. Soc. Faraday Trans. **89**, 4069 (1993).
[24] J. Corner, Proc. R. Soc. London, Ser. A **192**, 275 (1948).
[25] B. J. Berne and P. Pechukas, J. Chem. Phys. **56**, 4213 (1972).
[26] A. J. Stone, Mol. Phys. **36**, 241 (1987).
[27] J. A. C. Veerman and D. Frenkel, Phys. Rev. A **41**, 3237 (1990).
[28] J. A. Barker and R. O. Watts, Chem. Phys. Lett. **3**, 144 (1969).
[29] N. Metropolis, A. W. Rosenbluth, M. N. Rosenbluth, A. H. Teller, and E. Teller, J. Chem. Phys. **21**, 1087 (1953).
[30] M. P. Allen and D. J. Tildesley, *Computer Simulation of Liquids* (Clarendon, Oxford, 1987).
[31] L. Verlet, Phys. Rev. **165**, 201 (1968).
[32] C. Zannoni, in *The Molecular Physics of Liquid Crystals*, edited by G. R. Luckhurst and G. W. Gray (Academic, New York, 1979), Chaps. 3 and 9.
[33] A. Perera and G. N. Patey, J. Chem. Phys. **91**, 3045 (1989).
[34] J. Talbot, A. Perera, and G. N. Patey, Mol. Phys. **70**, 285 (1990).